GNSS multipath error model for airport surface operations

Leslie Montloin, Laurent Azoulai, Adrien Chen, Anaïs Martineau, Carl Milner, Alexandre Chabory, Christophe Macabiau

A GNSS Multipath Error Model for Airport Surface Operations

Leslie MONTLOIN, Laurent AZOULAI, Adrien CHEN, *Airbus, Toulouse, France*
Anaïs MARTINEAU, Carl MILNER, Alexandre CHABORY, Christophe MACABIAU, *ENAC Telecom Lab, Toulouse, France*

BIOGRAPHIES

Leslie MONTLOIN has a Master degree in electronic from the ENAC (French National School for Civil Aviation). Since 2011, she is a PhD student in the Signal Processing and Navigation Research Group (SIGNAV) of ENAC in Toulouse, France. The PhD project is in collaboration with the radio navigation systems department of Airbus. She is currently working on multipath modeling for taxi and parking operations.

Laurent AZOULAI graduated in 1996 of Institut Supérieur de l'Electronique de Paris as an engineer specialized in automatic systems. He is GNSS-Landing Systems Technical Expert within Airbus His activities focus on Approach and Landing and the use of GNSS in Communication, Navigation and Surveillance Airbus aircraft systems. He is involved in standardization activities dealing with GBAS Cat 2/3, GPS/Galileo and SBAS for which he is co-chairman of RTCA SC-159 SBAS Working Group.

Dr. Adrien CHEN graduated as an electronics engineer in 2007 from the ENAC in Toulouse, France. He received his Ph.D in 2010 related to GPS multipath prediction for airport navigation. He is currently a Navigation System Designer in Airbus.

Dr. Anaïs MARTINEAU graduated in 2005 as an electronics engineer from the Ecole Nationale de l'Aviation Civile (ENAC) in Toulouse, France. Since 2005, she has been working at the signal processing lab of the ENAC where she carries out research on integrity monitoring techniques. She received her Ph.D. in 2008 from the University of Toulouse.

Dr. Carl MILNER is an Assistant Professor within the Telecom Lab at the Ecole Nationale Aviation Civile. He has a Master's degree in Mathematics from the University of Warwick, a PhD in Geomatics from Imperial College London and has completed the graduate trainee programme at the European Space Agency. His research interests include GNSS augmentation systems, integrity monitoring, air navigation and applied mathematics.

Dr. Alexandre CHABORY graduated in 2001 as an electronics engineer from the French Civil Aviation University (ENAC). From 2001 to 2004, he was a PhD student with ONERA. From 2004 to 2007, he was a postdoctoral scientist with the Eindhoven University of Technology (TU/e). Since 2007, he is an assistant professor with the Electromagnetics and Antennas Research Group of the Telecom lab of ENAC. His research interests mainly deal with electromagnetic theory, modeling and applications.

Dr. Christophe MACABIAU graduated as an electronics engineer in 1992 from the ENAC in Toulouse, France. Since 1994, he has been working on the application of satellite navigation techniques to civil aviation. He received his PhD in 1997 and has been in charge of the signal processing lab of ENAC since 2000

ABSTRACT

The Global Navigation Satellite System (GNSS) is a worldwide position and time determination system currently used in civil aviation to support En-route to Precision Approach (PA) operations. Extending the use of GNSS to aircraft guidance during surface operations remains a challenge. Indeed, during taxi and parking operations, GNSS pseudo range measurements suffer from higher multipath errors than whilst in flight because of signal reflections from the aircraft structure, and from additional sources of multipath, such as the ground and obstacles surrounding the airborne antenna [2]. This can result in horizontal positioning errors that reach several meters [3]. The multipath ranging error model currently standardized for En-route to PA operations [8] is not designed to protect users from the effects of multipath from the ground and obstacles in airport environments. Hence, it is necessary to develop a multipath ranging error model adapted to airport environments in order to protect the user from the effects of multipath during surface operations (taxi and parking) and possibly correct these effects. Several steps are needed to set up such a model. The first step, which is the main objective of this paper, is to provide an analysis of the error on the raw code and smoothed code GPS L1 C/A pseudo range measurements due to multipath from:

- the aircraft structure and the ground,
- the aircraft structure, the ground, and a single obstacle surrounding the airborne antenna,

in both static and dynamic configurations.
Firstly, the analytical models of the raw and smoothed errors in the time domain assuming that the aircraft and the satellite are both static are provided. The derived models are parameterized by a time-independent, space-dependent coefficient. The physical meaning of this coefficient is provided, and its variation in the space domain is investigated. This coefficient is statistically modeled and over-bounded by a non-zero Gaussian distribution in the case where the pseudo range measurement is affected by multipath from the ground, the aircraft structure and a single obstacle. The influence of the type of obstacle and of the satellite elevation angle on the mean and the standard deviation of the Gaussian distribution are analyzed. A mathematical model of the variation of the standard deviation as a function of the elevation angle for a given obstacle is proposed.
Secondly, the definition of "dynamic regime" is discussed. The models of the raw code and smoothed code multipath ranging errors affecting an aircraft that performs a straight line trajectory with a constant speed in this airport are provided. In the case where the pseudo range measurement is affected by multipath from the ground, the aircraft structure and a single obstacle, these errors are over bounded by a stationary non-zero mean Gaussian distribution. The influence of the obstacle, the elevation angle and the aircraft dynamic on the Gaussian distribution mean and standard deviation are analyzed.

INTRODUCTION

The GNSS is currently used in civil aviation to provide aircraft with position and velocity estimates from En-route to Precision Approach (PA) operations. The challenge in the coming years is to extend the use of GNSS "from gate to gate" [4], and more particularly to aircraft guidance during surface operations and to automatic taxi and parking operations. One of the main issues in extending the use of GNSSs to surface operations is multipath. Multipath is the reception of echo replicas of the desired signal by the GNSS airborne antenna. For En-route to PA operations, the structure of the aircraft itself is the dominant source of multipath error. Multipath errors resulting from the aircraft structure have been widely investigated and over-bounded by a standardized model that is currently used in civil aviation GNSS integrity monitoring algorithms. However, during taxi and parking operations, additional sources of multipath errors may affect the pseudo-range measurements [6] and the integrity of the pseudo-range estimates. These additional sources of multipath are the ground, which can be modeled in airport environments by tar or grass to represent taxiways, and obstacles on the ground surrounding the GNSS airborne antenna such as aircrafts and buildings. This results in two main consequences. Firstly multipath replicas are one of the dominant contributors of error for surface operations. Secondly the standardized model used from En-route to PA operations is not valid for taxi and parking operations. Hence, it is necessary to develop a pseudo-range multipath error model specific to taxi and parking operations.
Few models have been proposed in the literature to predict multipath ranging errors in airport environments. Among these models there are:

- Mainly or purely **statistical models** which are based on extensive measurement campaigns. As an example, [7] uses the statistical transmission channel model developed in [20] to propose a multipath ranging error model in urban environment. The model proposed in [7] is used in some publications to bound the raw code multipath errors affecting pseudo-range measurements during surface operations. The main advantage of this kind of model is that they are independent on the considered airport. They are thus easy to embed since they do not require embedding airport database on board. However, some characteristics of the urban and airport environments are different. Hence urban statistical multipath ranging errors models do not seem well-adapted to precisely bound the multipath errors affecting the pseudo-range measurements in airport environments.
- Mainly or purely **deterministic models** which are based on an electromagnetic description of multipath. As an example, [6] provides a prediction of the multipath ranging error knowing a description of the 3D airport environment, the GNSS airborne antenna position and the satellite position. The main advantage of these models is the precision of the error prediction. The main limitation being the complexity of implementation requiring a realistic 3D representation of the airport environment.

The final objective of our work is to propose a multipath ranging error model that combines the ease of implementation of the statistical model and the precision of the predicted errors proposed by the deterministic model. More specifically, the final goal is to develop a model that allows protecting the user from the effects of multipath during taxi and parking operations while requiring a basic and simple 3D model of the airport. In order to achieve the final goal, it is important to determine the impact of the sources of multipath on the ranging errors. Hence, the main goal of this paper is to model the multipath ranging errors due to sources of multipath affecting GNSS pseudo range measurements during taxi and parking operations. Note that this paper focuses on GPS L1 C/A pseudo range error models. This paper is organized as follows:

- The **first section** provides a brief background on the impact of echo signals on GNSS receivers. This part also introduces the notations and the values of the GNSS receiver parameters used to perform the simulations whose results are presented in the paper.
- The **second section** provides the models of the multipath ranging error due to sources of multipath that are present during taxi and parking operations in static and dynamic configurations. More specifically, two kinds of models are derived: a model of the ranging error due to the reflection of the signal on the ground and the aircraft structure, and a model of the ranging error due to the reflection of the signal on the ground, on the aircraft structure and on a single obstacle surrounding the GNSS airborne antenna. This last model is driven by a parameter that depends on the type of obstacle and on the elevation angle. This second Section explains how the parameter is obtained for a single obstacle and a single elevation angle. The example of a 10m metallic obstacle at 35° elevation angle is taken.
- The **third section** provides numerical values of the multipath ranging error models parameters in static and dynamic configurations for different obstacles and for different elevation angles. The parameters have been obtained based on simulations performed with the multipath ranging error simulator presented in [21]. This simulator predicts code multipath ranging errors knowing the 3D environment, the satellite and the airborne antenna positions. It consists in a multipath generator and a GPS receiver simulator. GNSS multipath are generated using a method based on Physical Optics (PO).
- Finally, the main results derived in this paper and future works are presented in the **conclusion**.

I. BACKGROUND AND SIGNAL MODEL

This section aims to provide a general background on the impact of multipath on GNSS receivers and to introduce the notations that will be used. At first, the general architecture of the signal processing part of a GNSS receiver is provided in Fig. 1. In this Figure, DLL stands for Delay Locked Loop and PLL stands for Phase Locked Loop. Note that the operation of each block presented in Fig. 1 is detailed in [5].

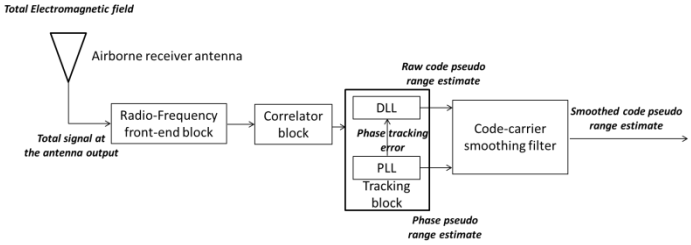

Figure 1: signal processing blocks of a GNSS receiver

Assuming that N echo signals are received by the airborne GNSS antenna at time t_k, the total (direct and echo) GPS L1 C/A signal at the output of the antenna at $t = t_k$ from satellite "i" can be modeled by Equation (1). Note that, for the sake of clarity, indices "i" are dropped in **Eq.1**:

$$s_{total}(t_k) = \alpha_0(t_k)c(t_k - \tau_{direct}(t_k)) \times \cos\left(2\pi\left(f_{L1} + f_{D,direct}(t_k)\right)\left(t_k - \tau_{direct}(t_k)\right) + \varphi_0\right) + \sum_{j=1}^{N} \alpha_j(t_k)c\left(t_k - \tau_{echo,j}(t_k)\right) \times \cos\left(2\pi\left(f_{L1} + f_{D,echo,j}(t_k)\right)\left(t_k - \tau_{echo,j}(t_k)\right) + \varphi_0\right) \quad \textbf{Eq.1}$$

where:

- $c(.)$ refers to the product between the GPS L1 C/A navigation message and spreading signal,
- $\alpha_m(t_k), m \in [\![0, N]\!]$ is the amplitude of the direct and echo signals at time $t = t_k$,
- $\tau_{direct}(t_k)$ [s] and $f_{D,direct}(t_k)$ [Hz] are the code delay and Doppler frequency of the direct signal at time $t = t_k$,
- $\tau_{echo,j}(t_k)$ [s] and $f_{D,echo,j}(t_k)$ [Hz] are the code delay and Doppler frequency of the j^{th} echo signal at time $t = t_k$, respectively,
- φ_0 is the initial phase of the carrier [rad],
- f_{L1} is the GPS L1 C/A carrier frequency [Hz].

Due to the presence of the N echo signals, the correlation function between the received signal and the locally generated signal becomes the sum of the ideal correlation function and a second version of the ideal correlation function that is scaled in amplitude, rotated in phase, and delayed [5]. Hence the composite correlation function may become asymmetrical in the presence of echo signals. This asymmetry generates an error on the code delay of the direct signal that is estimated by the DLL of the receiver. In the following, this error is called raw code multipath ranging error and is denoted as $\varepsilon_{code\ multipath}(t_k)$. The raw code and phase multipath ranging errors generate an error on the smoothed code pseudo range estimate at the code-carrier filter output, called smoothed code multipath ranging error and denoted as $\varepsilon_{smoothed\ multipath}(t_k)$ in the following. Since only raw code and smoothed code pseudo range estimates are used in civil aviation to evaluate the navigation solution [8], [9], [10], this document does not deal with phase multipath ranging errors. Note also that both raw and smoothed code pseudo range estimates are represented in Fig. 1.

Both raw and smoothed multipath ranging errors depend on the characteristics of the signal processing blocks of the GNSS receiver. Since this publication deals with GNSS multipath errors for civil aviation application, typical values of the parameters used in airborne GNSS receivers have been selected for the rest of the paper and are provided in Table 1 [6]. The sensitivity of the derived

error models to these parameters is not presented in this document and this analysis is left as future work.

Table 1: values of the GNSS receiver parameters considered for the characterization of the code and smoothed multipath ranging error

Block	Parameter	Type or value
Airborne receiver antenna	Antenna type	Realistic GPS antenna. The multipath on the aircraft structure are included in the radiation pattern of the antenna. The relative delays of the aircraft structure multipath are not taken into account in our error model. Indeed, it has been shown in [6] that they are not significant w.r.t the GPS L1 C/A chip period.
Radio-Frequency front-end block	Bandwidth of the front-end filter	20MHz
Tracking block	PLL aided DLL	yes
	DLL discriminator / PLL discriminator	Early minus Late Power / Arctangent
	Early-Late chip spacing	0.5 chips
	DLL bandwidth / PLL bandwidth	1Hz / 10Hz
	DLL and PLL order	2
	$f_s = 1/T_s$ sampling frequency of the code/ phase pseudo range estimates	5 Hz
Code-carrier smoothing filter	T_{smooth} time constant of the smoothing filter	100s

In this publication, the ground is modeled as a horizontal plane. The X and Y axes belong to this plane, are orthogonal and the X axis points in the North direction. O is the origin of the direct and orthogonal reference frame (O,X,Y,Z) that is depicted in Fig. 2, where Z is the local vertical vector pointing upwards. The azimuth angle is the angle between the X axis and the projection of the vector between the airborne antenna and the satellite on the (OXY) plane.

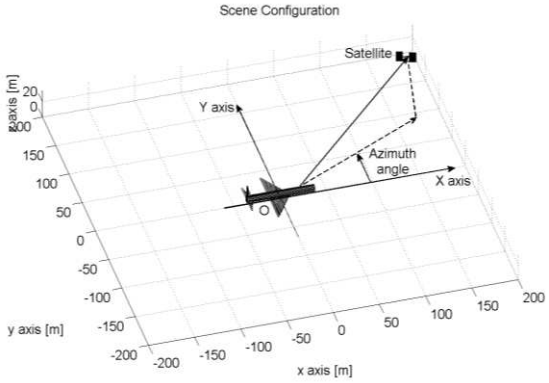

Figure 2: scene configuration

The following section aims to provide a model of the raw code and smoothed code multipath ranging errors in both static and dynamic configurations.

II. MULTIPATH RANGING ERROR MODELS

[6] and [11] underline the impact of aircraft dynamics on the multipath ranging errors affecting the raw and smoothed code pseudo range estimates. For this reason, static and dynamic configurations are treated separately in this research. The following subsection deals with multipath ranging errors model in static conditions.

II.1. Static Case

II.1.1. Variation of the error in the time domain

In this subsection, the evolution of the raw and smoothed code multipath ranging errors in static conditions as a function of time is investigated. Let's assume that the aircraft centerline is parallel to X axis, points to the North, and that the aircraft center is located at the origin of the (OXYZ) reference plane, as represented in Fig. 2. The azimuth angle of satellite "i" is set to 0° and the elevation angle is 20°. Let's assume that the pseudo range measurement between satellite "i" and the airborne antenna is suddenly affected by a multipath at $t_k = 0$s. Both raw and smoothed code multipath ranging errors are thus equal to 0m at $t_k = 0$s. From $t_k = 0$s, it is assumed that the aircraft, the satellite and the multipath error sources are static. Hence, the multipath parameters are constant in the time domain. The evolution of the raw and smoothed code multipath ranging errors as functions of time is represented in Fig. 3.

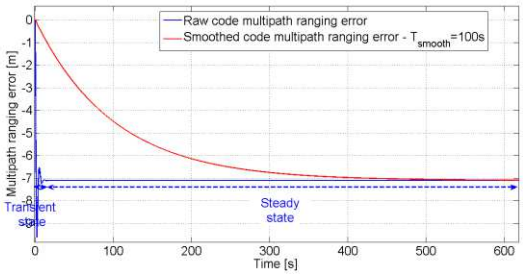

Figure 3: raw and smoothed code multipath ranging error due to the ground and the aircraft itself as a function of the time

Let's analyze the evolution of the raw code ranging error $\varepsilon_{\text{code multipath}}(t_k)$ (blue curve) as a function of time. From Fig.3, the impact of the multipath that appears at time $t_k = 0$s on the code multipath ranging error in steady state is $b = -7.1$m. Note that b is constant in the time domain since, from $t_k = 0$s, it is assumed that the aircraft, the satellite and the multipath error sources are static. From Table 1, the order of the implemented DLL is 2. Hence, the raw code multipath ranging error is the response of the time constant bias $b = -7.1$m to an equivalent 2nd order low-pass filter. Simulations have shown that the duration of the transient state of such a filter is roughly equal to 10s. In steady state, the raw code ranging error remains constant in the time domain $\varepsilon_{\text{code multipath}}(t_k) = b$. Note that the initial value of the raw code ranging error has to be adjusted depending on the situation. As an example, let's assume that the aircraft is at the gate. At this position, the raw code pseudo range measurement is affected by the multipath error b in steady state. The receiver is switched on. Let's note b' the code multipath ranging error at the acquisition block output. In this situation, the first raw code multipath ranging error at the DLL output is b', and then this error converges to the raw code multipath ranging error in steady state b.

Let's analyze the evolution of the smoothed code ranging error $\varepsilon_{\text{smoothed multipath}}(t_k)$ (red curve) as a function of time. In **APPENDIX A**, it is demonstrated that the raw code and smoothed code multipath ranging errors are related by:

$$\varepsilon_{\text{smoothed multipath}}(t_k) = \exp\left[-\frac{t_k}{T_{\text{smooth}}}\right]\left[c + b\left[\exp\left[\frac{t_k}{T_{\text{smooth}}}\right] - 1\right]\right] \quad \textbf{Eq.2}$$

where $c = \varepsilon_{\text{smoothed multipath}}(t_k = 0)$. Note that, as for the raw case, the value of c depends on the situation. Note also that, as underlined in [17], during the first T_{smooth} seconds after a cold start or a new start following a loss of lock of the GNSS signal, the coefficients of the code-carrier smoothing filter implemented in some airborne GNSS receivers vary in the time domain, leading to change the shape of the red curve and its analytical expression. However, in this paper, it is assumed that the implemented code-carrier smoothing filter is the reference filter presented in Section 2.1.4.1.1 of [8] and in **APPENDIX A** of this paper. In the presence of the reference filter, Equation (2) is always valid since the coefficients of the reference filter do not vary during the first T_{smooth} seconds after a cold start or a new start following a loss of lock of the GNSS signal.

To conclude, in the time domain, as both DLL and smoothing filters can be considered as 2nd order and 1st order low-pass filters, respectively, both raw and smoothed code ranging errors converge to the DLL output code multipath ranging error in steady state, denoted as b . The response time of the DLL is few seconds, and the response time of the smoothing filter is a function of the constant time of the smoothing filter. The next paragraph aims to describe the spatial variation of b in the airport environment.

II.1.2. Variation of the error in the space domain

During taxi and parking operations, three main sources of multipath have been distinguished:

- The **aircraft structure**. From Table 1, the impact of the structure of the aircraft on the multipath ranging errors is taken into account in the radiation-pattern of the GPS airborne antenna model used in the GPS multipath ranging error simulator.
- The ground which is modeled by dry tar of relative permittivity of $2 - j0{,}12$ to represent a taxiway [6]. The imaginary part of the relative permittivity represents losses.
- The **obstacles surrounding the GNSS airborne antenna**, such as vehicles, buildings and other aircraft in the airport. In this publication, simulations have been performed assuming that obstacles are metallic, concrete and glass cubes of size in the range [1m,20m]. Note that the façade of the considered obstacles are assumed to be smooth and homogeneous.

During taxi and parking operations, the k pseudo range measurements used by the GNSS airborne receiver to estimate the navigation solution are all affected by echo signals from the ground and the aircraft structure. However, over the k pseudo range measurements, $k - m$ (with $m \in [\![0, k]\!]$ is the number of measurements only affected by the aircraft structure and the ground), measurements are also affected by echo signals from obstacles surrounding the GNSS airborne antenna, depending on the relative position of the satellites, the airborne antenna and the obstacles in the airport. Note that, in this paper, each pseudo range measurement cannot be affected by more than a single obstacle, and the case where a pseudo range measurement is affected by two or more obstacles at the same time is not considered. Note that airports have general properties in common. On one side of the taxiways and parking areas there are the

runways and on the other sides there are the airport buildings [6]. Hence, a first approach reveals that pseudo range measurements are not likely to be affected by more than a single obstacle. However, this hypothesis must still be validated. Finally, interactions up to order 1 are considered in this paper. In other words, the echo signals at the antenna input are replicas of the direct signal reflected from only one source of multipath. As a consequence, and as an illustration, echo signals reflected from one obstacle and then from the ground are not considered in this publication.

Two different raw and smoothed code multipath ranging error models are presented in this paper:

- The first one models the ranging error due to the aircraft structure and the ground (see section **II.1.2.1**),
- The second one models the ranging error due to the aircraft structure, the ground and a single obstacle (see section **II.1.2.2**).

II.1.2.1. Aircraft structure and ground induced error in the space domain

II.1.2.1.1. Variations of b in the space domain

This paragraph aims to describe the spatial variation of the raw code multipath ranging error b due to the ground and the aircraft structure in the airport environment. Let's note $b = b_{A/C+ground}$ in this case. Note that, since the impact of the aircraft structure is included in the antenna radiation pattern, in our signal model, the airborne antenna receives only two signals from the considered satellite in this case: the direct signal and the 1st echo that is the direct signal reflected from the ground, and that is represented by index "1" in the following equations.

It can be easily demonstrated that the relative code delay between the echo signal from the ground and the direct signal is given by :

$$\Delta\tau_1(x_n) = \tau_{echo,1}(x_n) - \tau_{direct}(x_n) = 2.h_{ant}.\sin(El) \quad \textbf{Eq.3}$$

where:

- The antenna height with respect to the ground is denoted as h_{ant},
- El is the elevation angle.

From Equation (3), it can be already expected that the relative code delay $\Delta\tau_1$, and thus the relative phase delay $\Delta\phi_1$, will remain roughly constant over the airport scale since the angular variations of the elevation angle El at the scale of the airport will not be significant. Table 2 aims to quantify the maximal variations of $\Delta\tau_1$ and $\Delta\phi_1$, along a 1km segment parallel to the X axis. Along the segment, the aircraft centerline is parallel to X axis and points to the North. The azimuth angle of the satellite is set to 0° and the elevation angle is $El = 20°$. The antenna height is $h_{ant} = 8.10m$ for the considered aircraft.

Table 2: maximal variation of the multipath parameters along a 1000m segment in the airport

Multipath parameter	**Deviation between the minimal and maximal value along a 1km segment**
$\Delta\tau_1 = \tau_{echo,1} - \tau_{direct}$	$7{,}3.10^{-13}\ s \ll \frac{C_s}{2}$
$\Delta\phi_1 = -2\pi f_{L1}\Delta\tau_1$	$7{,}2.10^{-3}\ rad$

From Table 2, as expected, the relative code delay and phase parameters can be considered as constant along the segment. Simulations have shown that the amplitude of the direct and echo signal also remains roughly constant over the segment. The multipath parameters ($\Delta\tau_1$, $\Delta\phi_1$ and the amplitude ratio between the echo signal and the direct signal $= \frac{\alpha_1}{\alpha_0}$) determine the value of the DLL output multipath code ranging error in steady state $b_{A/C+ground}$. Since the multipath parameters are considered as constant over the segment, $b_{A/C+ground}$ can be considered as roughly constant along the segment. As an illustration, the difference between the minimum and maximum $b_{A/C+ground}$ is 1.2 mm. Simulations have shown that this result can be extended to the airport surface where $b_{A/C+ground}$ remains roughly constant for fixed elevation, azimuth angles, and orientation of the aircraft in the airport.

II.1.2.1.1. Model of b in the space domain

Note that the relative code delay and the relative phase between the direct signal and the signal reflected from the ground depend on the elevation angle. In addition, the amplitudes of the direct and echo signals, α_0 and α_1 , at the antenna output depend on the elevation angle and on the relative angle between the azimuth angle and the orientation of the aircraft in the airport. This is because the GPS airborne antenna pattern model is strongly anisotropic. Hence, $b_{A/C+ground}$ depends on the satellite elevation angle and on the relative angle between the azimuth angle and the orientation of the aircraft in the airport.

We have simulated the values of $b_{A/C+ground}$ for a wide range of elevation and azimuth angles and we have obtained the following results. For a fixed relative angle between the azimuth angle and the orientation of the aircraft, the magnitude of $b_{A/C+ground}$ is a few mm up to few cm from 90°elevation angle to 35° elevation angles. It increases between 35° and 20° elevation angles and reaches a few dm (roughly 30cm) at 20° elevation angle. For a fixed elevation angle above 30°, when the relative angle between the azimuth angle and the orientation of

the aircraft changes in the range $[0,2\pi]$,the magnitude of $b_{A/C+ground}$ varies of few mm. For an elevation angle below 30°, the magnitude of $b_{A/C+ground}$ varies by a few cm with the relative angle between the azimuth angle and the orientation of the aircraft. To conclude $b_{A/C+ground}$ does not depend so much on the azimuth angle of the satellite and on the aircraft orientation. $b_{A/C+ground}$ is very sensitive to the variations of the elevation angle.

II.1.2.2. Aircraft, ground and obstacle induced error in the space domain

II.1.2.2.1. Variations of the aircraft, ground and obstacle induced error in the space domain

This paragraph describes the spatial variation of the raw code multipath ranging error b due to the ground, the aircraft structure and a single obstacle in the airport environment. Let's note $b = b_{A/C+ground+obs}$ in this case.

In order to investigate the variation of $b_{A/C+ground+obs}$ in the space domain, it is proposed to investigate the variation of $b_{A/C+ground+obs}$ along a segment [AB] of the airport. The X coordinates of A and B are x_0 and x_f, respectively. [AB] is selected to be in the impact zone of the 10m metallic cubic obstacle. In this paper, the impact zone is defined as the area where the raw code multipath ranging errors induced by multipath from the illuminated façade of the obstacle is significant with respect to the error due to multipath from the aircraft structure and the ground. From section **II.1.2.1.1,** ranging errors due to multipath from the aircraft structure and the ground are few mm to few cm above 35° and are few cm to few dm between 20° and 35° elevation angles. Hence:

- From 35° to 90° elevation angles, the impact zone is defined as the area where the amplitude of the errors due to the obstacle is above 1cm,
- From 20° to 35° elevation angles, the impact zone is defined as the area where the amplitude of the errors due to the obstacle is above 10cm.

The location and dimension of the impact zone mainly depend on the dimensions, shape and material of the obstacle and on the elevation angle of the satellite. [AB] is orthogonal to the scattered façade of the cube. Both segment [AB] and impact zone are indicated in Fig.4. The façade of the building, which is represented by a 10m cube, is parallel to the Y axis and the azimuth angle of the satellite is set to 0°. The elevation angle is 35°. The aircraft centerline is parallel to the X axis.

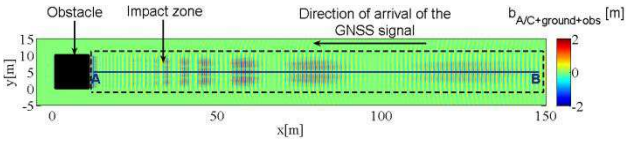

Figure 4: Impact zone of a 10m cubic metallic obstacle and [AB] segment in the impact zone

$b_{A/C+ground+obs}$ is represented along a portion of [AB] in Fig. 5.

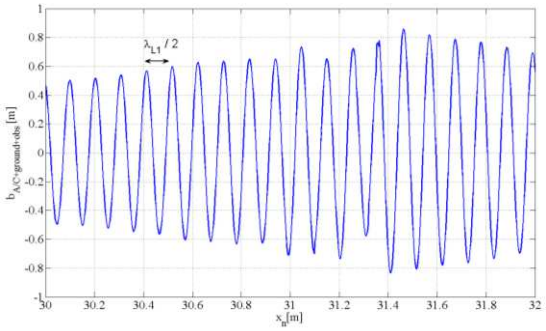

Figure 5: Evolution of $b_{A/C+ground+obs}$ along a portion of [AB] – elevation angle = 35°, azimuth angle = 0°, illuminated façade parallel to the Y axis, aircraft centerline parallel to the X axis and points in the North direction

The strong variations of $b_{A/C+ground+obs}$ along [AB] are interpreted as follows. Let's simplify the problem by assuming that the airborne antenna receives 3 signals: the direct signal characterized by a code delay τ_{direct}, the signal reflected by the ground characterized by a code delay $\tau_{reflect,1}$, and only one signal reflected from the façade and characterized by a code delay $\tau_{reflect,2}$. Let's state $\tau_{A\rightarrow obs}$ the time of propagation between A and the façade of the building. The code delay difference between the signal reflected from the façade and the direct signal when the airborne antenna is in$x_n, x_n \in [x_0, x_f]$, is given by:

$$\Delta\tau_2(x_n) = \tau_{reflect,2}(x_n) - \tau_{direct}(x_n) = 2\tau_{A\rightarrow obs} + \frac{2}{c}(x_n - x_0) \quad \textbf{Eq.4}$$

From **Eq.4**, it is deduced that 2 points on [AB] separated by a distance of $\frac{\lambda_{L1}}{2} \approx 10$cm have the same modulo 2π relative phase $\Delta\phi_2$. The small scale variations of the relative phase along [AB] causes small scale variations (spatial period of $\frac{\lambda_{L1}}{2}$) of $b_{A/C+ground+obs}$ along [AB], as observed in Fig. 5. Note that the analytical expression of $b_{A/C+ground+obs}$ along [AB] is provided in **APPENDIX B** for an Early minus Late power DLL discriminator and by considering only multipath from the illuminated façade. Note also that, as depicted in Fig. 4, $b_{A/C+ground+obs}$ is contained within an error envelope that presents large lobes of few meters length along [AB]. Further details

about the shape of the error envelope along [AB] are provided in [12] [5].

To conclude with, $b_{A/C+ground+obs}$ presents strong amplitude variations in the impact zone. Determining the value of $b_{A/C+ground+obs}$ in a deterministic way is complex as [6]:

- It would require knowing $b_{A/C+ground+obs}$ at each point of the impact zone, which is particularly difficult to assess due to the large number of parameters influencing the oscillations and values of $b_{A/C+ground+obs}$ in the impact zone (elevation angles, orientation of the façade of the building with respect to the direction of propagation of the GNSS signal, exact characteristics of the obstacle, etc.)
- It would require knowing the position of the airborne antenna in the impact zone with a high level of precision (cm precision level).

For these reasons, providing a statistical characterization of $b_{A/C+ground+obs}$in the impact zone is required. This technique allows removing the dependence of the $b_{A/C+ground+obs}$ values to the position of the airborne antenna in the impact zone.The statistical properties of the multipath ranging errors in airport environments have already been exploited in [6] in order to determine the risky areas of the airport, that is to say the areas where the ranging errors are significant. In this paper, it is proposed to investigate and model the statistical distribution of $b_{A/C+ground+obs}$ in the impact zone of the obstacle in order to get a simple model of the error in the impact zone of the obstacle. This is the goal of next section.

II.1.2.2.2. Model of the aircraft, ground and obstacle induced error in the space domain

In order to characterize the statistical distribution of $b_{A/C+ground+obs}$ in the impact zone of an obstacle, a large number of $b_{A/C+ground+obs}$ values have been randomly computed in the impact zone of several kinds of obstacles thanks to the multipath ranging error simulator presented in [6]. Then, the Probability Density Functions (PDFs) related to the distributions of $b_{A/C+ground+obs}$ values have been considered. As an example, Fig. 6 depicts the PDF that corresponds to the distribution of $b_{A/C+ground+obs}$ values in the impact zone of the 10m metallic cube (blue curve).

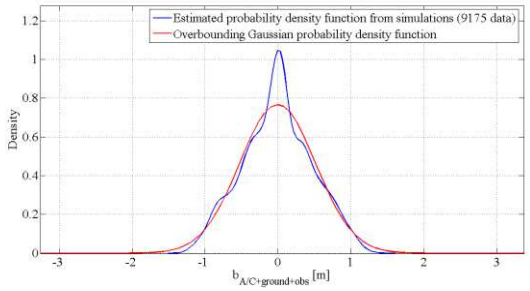

Figure 6: PDF of the estimated distribution of $b_{A/C+ground+obs}$ from simulations in the impact zone of a 10m metallic cube, elevation angle = 35°, azimuth angle = 0°, illuminated façade parallel to the Y axis, aircraft centerline parallel to the X axis, and PDF of the over-bounding Gaussian distribution

In order to find the statistical distribution that best fits the estimated distribution depicted in Fig. 6, blue curve, QQplots between the estimated distribution and classical distributions have been plotted and compared. It has been found that, for all selected elevation angles (15°, 20°, 35°, 50°, 65°, 80°), Gaussian mixture distributions best fit the estimated distribution. Note that the algorithm used to fit the estimated distribution by Gaussian mixture distributions is called Expectation Maximization [13]. The Gaussian mixture distribution is quite complex to manipulate since it requires knowing the weight, the mean and the standard deviation of each Gaussian component of the Gaussian mixture distribution. In addition, the Expectation Maximization algorithm is not designed to produce Gaussian mixture distributions that over-bound the tails of the estimated distributions. The multipath ranging error model proposed in this document is intended to be included within GNSS integrity monitoring algorithms for airport operations. For this reason, it appears to be more judicious to over-bound the estimated distributions by a single Gaussian distribution. To do that, DeCleene's Cumulative Density Function (CDF) algorithm is used [14]. CDF method assures that,$\forall x \epsilon \mathbb{R}^{+*}$, the estimated $P(|b_{A/C+ground+obs}| > x)$ is lower than $P(|\psi| > x)$, where $\psi \sim$overbounding Gaussian distribution.

Note that the CDF over-bounding method requires the estimated distribution to be symmetric and unimodal. The estimated distributions do not exactly fulfil these conditions, but approximately do. Moreover, CDF over-bounding method requires the estimated distribution to be zero-mean. Hence, the estimated distribution is at first centred, then the CDF over-bounding algorithm is applied to the centred distribution, and finally the mean μ_{static} of the estimated distribution is added to the obtained zero-mean overbounding Gaussian distribution $N(0, \sigma_{static})$.

The PDF of the over bounding Gaussian distribution for a 10m metallic building is represented in red in Fig. 6.

Numerically, a standard deviation of the estimated code ranging errors in the impact zone of 47.6 cm has been evaluated. Let's state $N(\mu_{static}, \sigma_{static})$ the over-bounding Gaussian distribution. In this example, $\mu_{static} = -6.2mm$, and corresponds to the impact of the ground and the aircraft itself on the code ranging error. The sigma of the over-bounding Gaussian distribution obtained with DeCleene's algorithm is $\sigma_{static} = 52cm$, which represents a small increase with respect to the standard deviation of the estimated errors.

II.1.3. Conclusion

In this section, it has been established that the errors affecting raw code and smoothed code pseudo range measurements in static configuration converge in the time domain to a time-independent parameter b, where:

- $b = b_{A/C+ground}$ when the pseudo range is affected by multipath from the aircraft structure and from the ground, and $b = b_{A/C+ground}$ is a constant term at the airport scale and only depends on the elevation, azimuth angles and orientation of the aircraft,
- $b = b_{A/C+ground+obs}$ when the pseudo range is affected by multipath from the aircraft structure, from the ground, and from a single obstacle, and $b = b_{A/C+ground+obs}$ is overbounded by a Gaussian distribution $N(\mu_{static}, \sigma_{static})$. Note that μ_{static} and σ_{static} depend on the obstacle, on the elevation angle, on the relative angle between the azimuth angle and orientation of the aircraft, and on the orientation of the façade of the obstacle with respect to the direction of propagation of the incoming GNSS signal.

II.2. Dynamic Case

This Section provides a model of the raw and smoothed code multipath ranging errors in the dynamic case. At first, let's discuss the concept of the "dynamic regime". In the airport environment, the total received signal at the antenna output is characterized by the channel through which the signal is propagated, namely the propagation channel [18]. Many elements influence the propagation channel [19] such as the environment in which the propagation takes place. When the aircraft moves along a trajectory in the airport, its environment changes, leading to variations of the coefficients of the propagation channel equivalent filter in the time domain. The rate of change of these coefficients depends on the aircraft speed along the trajectory. Fast variations of the coefficients along the trajectory change the way the DLL responds to the multipath along this trajectory. The minimal aircraft speed that leads to change the response of the DLL has to be established in order to clearly differentiate the "dynamic regime" from the "static regime". This minimal speed has not been derived theoretically for the following reason. From Table 2-17 of [15], the speed of the aircraft during taxi and parking operations is in the range [$1m.s^{-1}$,$10m.s^{-1}$]. At $1m.s^{-1}$, simulations have shown that the response of the DLL is already different from its response in the static configuration. Hence, in this publication, the speed threshold of the dynamic configuration comes from the operational constraints.

Note that, in this document, the case where the receiver has a constant speed is treated, and the case where the receiver has non-zero acceleration is not considered. Note also that curved trajectories are not treated in this publication. A first approach reveals that the exact shape of the trajectory in the impact zone is not likely to induce major changes in the error model results in the dynamic case. However, this hypothesis must still be validated. Finally, an important remark is that the motion of the satellite is not taken into account in the dynamic case. Indeed, the angular variation of the elevation angle is few tenths of degrees during trajectories of few seconds up to few minutes. Hence, in this Section, the satellite is assumed to be static when the aircraft performs its straight line trajectory.

II.2.1. Aircraft structure and ground induced error

From section **II.1.2.1**, it has been established that the code multipath ranging error in steady state is roughly constant over the airport and depends on the elevation angle and the relative angle between the azimuth angle and orientation of the aircraft. Along any straight line trajectory of the airport, the satellite is considered as static. Hence, the elevation angle and the relative angle between the azimuth angle and orientation of the aircraft are considered as roughly constant, and the raw code multipath ranging error in steady state remains roughly constant (equal to $b_{A/C+ground}$) over the trajectory. Therefore, after a transient time, the raw and smoothed code multipath ranging errors remain constant on the trajectory and thus in the time domain:

$$\varepsilon_{\text{code multipath}}(t_k) = \varepsilon_{\text{smoothed multipath}}(t_k) = b_{A/C+ground} \quad \textbf{Eq.5}$$

where $b_{A/C+ground}$ is defined in section **II.1.2.2.**

II.2.2. Aircraft structure, ground and obstacle induced error

II.2.2.1. Factors influencing the error along a trajectory

In section **II.1.2.2**, it has been established that the code multipath ranging error in steady state in the impact zone of an obstacle presents small scales variations (dm level) characterized by high amplitudes (cm to m level) over any segment of the impact zone. Hence, the raw and smoothed code ranging errors over any straight line trajectory belonging to the impact zone are also characterized by

small scale oscillations. Note two main factors impact the raw and smoothed code multipath ranging errors that affect an aircraft performing a straight line trajectory in the impact zone of an obstacle. Amongst these factors:

- The raw code multipath ranging errors in steady state (static case $b_{A/C+ground+obs}$errors) along the trajectory. Note that the $b_{A/C+ground+obs}$ values along the trajectory highly depend on the orientation and on the initial point of the trajectory.
- The aircraft dynamic that smoothes the variations of $b_{A/C+ground+obs}$ along the trajectory [6].

To conclude, the code ranging errors along a trajectory in the impact zone of an obstacle strongly depend on the location of the trajectory in the impact zone and on the aircraft dynamic. Determining the value of the code ranging errors in the dynamic configuration in a deterministic way is complex mainly because it would require knowing the trajectory of the aircraft in the impact zone precisely. Hence, and in order to remove the dependence of the errors along the trajectory to the trajectory location, it is proposed to investigate and model the statistical distribution of the errors along a large number of trajectories in the impact zone. This is the goal of the following subsection.

II.2.2.2. Model of the aircraft, ground and obstacle induced error

In order to investigate and model the statistical distribution of the multipath ranging errors in the impact zone, a large number of trajectories in the impact zone have been randomly simulated. This will allow representing all possible trajectories in the impact zone. Then, multipath ranging errors along these trajectories have been determined thanks to the multipath ranging error simulator [6]. In each simulation:

- The characteristics of each trajectory, i.e. the initial position and direction of the trajectories, are chosen randomly and independently each other,
- The aircraft speed along the trajectories is fixed,
- The orientation of the façade, the azimuth and elevation angles of the satellite are fixed,
- The characteristics of the obstacle (shape, size, materials) are fixed.

Then, the PDFs related to the distributions of the multipath ranging error values obtained by simulations along all computed trajectories have been considered. As an example, Fig. 7 depicts the PDF that corresponds to the distribution of the raw code multipath ranging error values $\varepsilon_{\text{code multipath}}(t_k)$ in the impact zone of the 10m metallic cube (blue curve). The speed of the aircraft in the impact zone is 5m.s^{-1}.

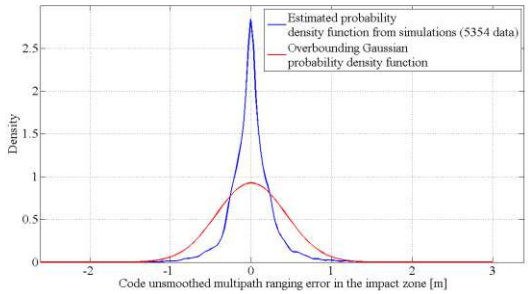

Figure 7: PDF of the estimated distribution of the code ranging error from simulations in the impact zone of a 10m metallic cube, elevation angle = 35°, azimuth angle = 0°, façade parallel to the Y axis, aircraft speed = 5m.s^{-1} and PDF of the over bounding Gaussian distribution

For the same reasons as those exposed in section **II.1.2.2.2**., it is proposed to over-bound the estimated distribution of the code ranging errors in the impact zone and in dynamic conditions by a single Gaussian distribution based on Decleene's CDF algorithm. Fig. 7 represents the PDF of the estimated distribution of the raw code multipath ranging error in the impact zone of the 10m metallic cube with an aircraft speed of 5m.s^{-1}, and the PDF of the over bounding Gaussian distribution obtained with DeCleene's CDF algorithm. Note that the red curve does not represent the narrow peak of the estimated distribution around zero, but has the advantage to overbound the tails of the estimated distribution. The feasibility to overbound the estimated distribution by a non-Gaussian law (such as an exponential law) that best fits the estimated distribution is left as future work.

Numerically, a standard deviation of the estimated code ranging errors in the impact zone of 26 cm has been evaluated. In this example, $\mu_{dyn} = 1.8\text{mm}$ and sigma of the overbounding Gaussian distribution obtained with DeCleene's algorithm is $\sigma_{dyn} = 43\text{cm}$, which represents a significant increase with respect to the standard deviation of the estimated code ranging errors determined in the impact zone.

II.2.3. Conclusion

In this section, it has been established that the raw and smoothed code multipath ranging measurements in dynamic configurations over a straight line trajectory are affected by a constant error $b = b_{A/C+ground}$ if the pseudo range is only affected by multipath from the ground and from the aircraft structure. If the pseudo range measurement is also affected by multipath from a single obstacle, the errors are over-bounded by single Gaussian distribution denoted as $N(\mu_{dyn}, \sigma_{dyn})$ in the following. Note that μ_{dyn} and σ_{dyn} depend on the obstacle, on the elevation angle, on the orientation of the façade of the

obstacle and of the aircraft with respect to the direction of propagation of the incoming GNSS signal, on the aircraft speed in the impact zone, and on the time constant of code-carrier smoothing filter, if $N(\mu_{dyn}, \sigma_{dyn})$ over-bounds the smoothed code multipath ranging errors in the impact zone.

III. SIMULATION RESULTS

In **II.1.2.1.2**, orders of magnitude of the code ranging errors due to multipath from the ground and from the aircraft structure have been provided. For this reason, this section focuses on errors due to multipath from the ground, from the aircraft structure, and from a single obstacle. The goal of this section is to provide the Gaussian distribution parameters μ_{static}, σ_{static} (see section **III.1**) μ_{dyn}, σ_{dyn} (see section **III.2**) for different kinds of obstacles and for different elevation angles. Obstacles considered in this section are metallic, concrete and glass cubic obstacles with sizes in the range [1m,20m]. Note that the façade of the considered obstacles are assumed to be smooth and homogeneous. The analysis of the influence of the orientation of the façade and of inhomogeneous and non-smooth façades on the simulation results is left as future works. The distribution parameters are given assuming that the illuminated façade is parallel to the Y axis and that the satellite azimuth angle is 0°. From section **II.1.2**, interactions up to order 1 are considered in this paper. In other words, the echo signals reflecting by more than one source of multipath (such as signals reflected from the obstacle and then from the ground) are not taken into account in the simulation results. The results are obtained with the multipath ranging error predictor described in [6]. More details about this simulator are provided in the Introduction part.

III.1. Static case

In this Section, it is assumed that the aircraft is static. The aircraft centerline is parallel to the X axis and points in the North direction. The azimuth angle is 0°.

III.1.1. Mean value μ_{static}

The means μ_{static} of the Gaussian distribution $N(\mu_{static}, \sigma_{static})$ that over-bounds the distribution of the code multipath ranging error $b_{A/C+ground+obs}$ in the impact zone of a 10m and of a 20m metallic building are provided in Fig. 8 and 9, respectively.

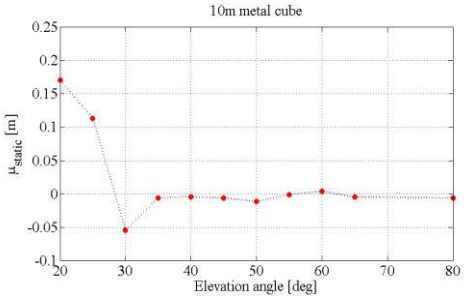

Figure 8: μ_{static} as a function of the elevation angle – impact zone of a 10m metallic cube

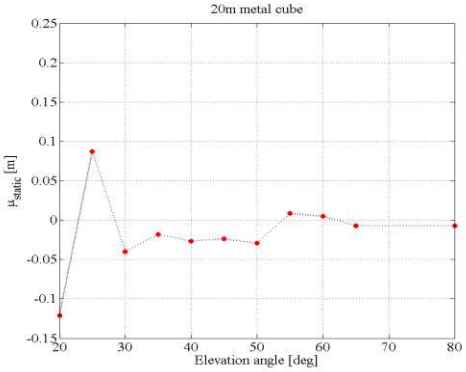

Figure 9: μ_{static} as a function of the elevation angle – impact zone of a 20m metallic cube

From Fig. 8 and 9, the distribution of the code delay error in steady state, $b_{A/C+ground+obs}$, is roughly centered for elevation angles equal and above 35° (mm and cm level). However, non-zero mean values (dm level) are observed for elevation angles below 35°. This can be interpreted as follows. Two causes are responsible for the non-zero mean errors observed at low elevation angles and. The causes are detailed below.

Multipath from the ground and from the aircraft structure are the first cause. For a fixed elevation angle, all points of the impact zone are affected by the same multipath from the ground and from the aircraft structure. This phenomena leads to shift the estimated PDF towards a non-zero value which is roughly equal to $b_{A/C+ground}$ at the corresponding elevation angle. This partly explains why μ_{static} is not zero at low elevation angles. As an example, at an elevation of 20°, the mean of the distribution is $\mu_{static} = 17$cm in the impact zone of a 10m metallic building, which corresponds to the contribution of the ground and of the aircraft structure for an elevation of 20°.

The shape of the error $b_{A/C+ground+obs}$ in the direction orthogonal to the illuminated façade is the second cause of the non-zero mean at low elevation angles. From Fig. **B.1** and **B.2** of **APPENDIX B**, $b_{A/C+ground+obs}$ along the direction orthogonal to the illuminated façade:

- Is roughly sinusoidal when the amplitude ratio between the echo signals from the façade and the direct signal is relatively low (Fig. **B.1**),
- Is almost always negative with sharp positive peaks when the amplitude ratio between the echo signals from the façade and the direct signal is relatively high (Fig. **B.2**).

Therefore, when the amplitude ratio is relatively high, the estimated distribution of $b_{A/C+ground+obs}$ presents more negative values than positive values.
From **APPENDIX C**, large obstacles, such as 20m metallic cube, induce high scattered field power in the impact zone. At low elevation angles, the scattered field is not as well rejected as for high elevation angles by the GPS antenna. Hence, in the impact zone of large buildings, and at low elevation angles, the ratio between the amplitudes of the echo signals from the building and of the direct signal is relatively high.
We can thus conclude that, at low elevation angle, and in the impact zone of large obstacles, $b_{A/C+ground+obs}$ presents more negative values than positive values, leading to non-zero μ_{static} values. At a fixed elevation angle, μ_{static} for a small obstacle is lower thanμ_{static} for a large obstacle.

III.1.2. Standard deviation value σ_{static}

The standard deviations σ_{static} of the Gaussian distribution $N(\mu_{static}, \sigma_{static})$ that over-bound the distribution of the code multipath ranging error $b_{A/C+ground+obs}$ in the impact zone of a 10m and of a 20m metallic building are provided in Fig. 10 and 11 (red points and dashed line), respectively.

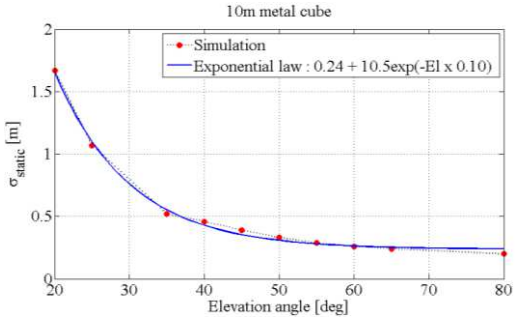

Figure 10: σ_{static} as a function of the elevation angle – impact zone of a 10m metallic cube

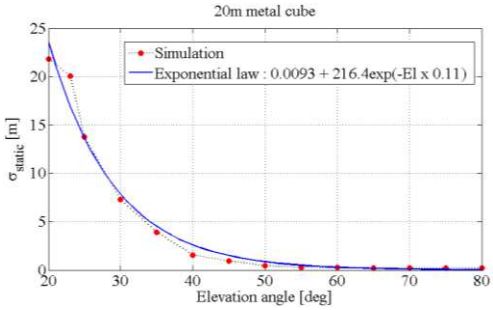

Figure 11: σ_{static} as a function of the elevation angle – impact zone of a 20m metallic cube

Note that the evolution of σ_{static} as a function of the elevation angle is fitted by an exponential function that has the following shape:

$$\sigma_{static,exp\ fitting}(El) = a_0 + a_1.\exp(-El.a_2) \qquad \textbf{Eq.6}$$

where a_0, a_1, a_2 are real values obtained by solving a system of N equations (N is the number of elevation angles for which a σ_{static} value has been obtained) with 3 unknowns. The coefficients depend on the type of obstacle. The exponential fitted curves are depicted in blue in Fig. 10 and 11. a_0, a_1, a_2 coefficients are provided in Table 3 for metallic, concrete and glass obstacles.

Table 3: coefficients of the exponential laws that fit the values of σ_{static} obtained by simulations

	Metallic obstacles			Concrete obstacles			Glass obstacles		
Size [m]	1	10	20	1	10	20	1	10	20
a_0	0.08	0.24	0.009	0.03	0.09	0.15	0.03	0.10	0.02
a_1	1.4	10.5	216.4	0.79	4.8	120.5	1.4	7.0	110.9
a_2	0.08	0.10	0.11	0.09	0.11	0.15	0.10	0.12	0.11

The value of coefficient $a_0$can be artificially increased in such a way that the exponential law over-bounds all estimated values of σ_{static}. Note also that the method to get the values a_0, a_1, a_2 shall be discussed. Deriving these coefficients by simulations requires using a GNSS multipath ranging error predictor software and is relatively time-consuming (few hours of simulation per obstacles). However, other methods, such as deriving the coefficients by data collection, seem to be worst in terms of cost, complexity and time. Indeed, it would require extracting the multipath errors from the GNSS measurements and measuring the multipath errors at several positions of the impact zone, and for several elevation angles.

From Fig. 10, 11, and From Table 3, the value of σ_{static} for a fixed elevation angle is smaller for the 10m metallic obstacle than for the 20m metallic obstacle. Hence the value of σ_{static} depends on the size of the obstacle. An interpretation of this observation is given as follows. The

Electromagnetic (EM) field scattered by small obstacles (size significantly below 10m) is quasi isotropic. Hence, the field scattered by small obstacles is spread in the airport surface towards different directions. The field scattered by large obstacles is more directional and the energy of the scattered field is focused around a single direction. This phenomenon is visualized in **APPENDIX C.** Therefore, the amplitudes of the signals reflected from the façade of the building are higher in front of large obstacles than in front of the small obstacles. High echo signal amplitudes induce variations of the code ranging error in the impact zone characterized by strong amplitudes. Hence the standard deviation of the code ranging error $b_{A/C+ground+obs}$, and thus the σ_{static} value, are larger for large obstacles than for small obstacles.

It is important to note that the exponential model for the variation of σ_{static} as a function of the elevation angle is only valid for elevations in the range $[20°, 90°]$. Indeed, for elevation angles in the range $[5°, 20°]$, strong negative mean values μ_{static} (few meters) and high standard deviation values of the code ranging error $b_{A/C+ground+obs}$ (few dozens of m) are observed in the impact zone of large metallic buildings. This can be interpreted as follows. At low elevation angles, the echo waves are mainly LHCP waves and are not rejected as well as for high elevation angles. This is because the right and left polarization components of the GPS realistic antenna pattern have the same order of magnitude, and the polarization of the real antenna is thus roughly linear at low elevation angles. In addition, large metallic obstacles generate high scattered field power in the impact zone. From **APPENDIX D**, both phenomena can make the amplitude of the signal reflected from the obstacle larger than the amplitude of the direct signal. As shown in **APPENDIX D**, this scenario is observed between 5m and 80 m from the façade of a 15m metallic building, at 5° elevation angle. In this situation, the GNSS receiver estimates the 1st echo code delay. Hence, the code delay error that corresponds to the difference between the true code delay and the estimated code delay is strongly negative in this situation. This explains why strong negative mean values μ_{static} (few meters) and high standard deviation values of the code ranging error $b_{A/C+ground+obs}$ (few dozens of m) are observed in the impact zone of large metallic buildings at low elevation angles (below 20°). The multipath ranging error model proposed in this document is intended to contribute to the basis for GNSS integrity monitoring algorithm for airport operations. Including low elevation angles in this model would lead to a model unsuitable for integrity purposes. For this reason, a multipath ranging error model for elevation angles in the range [20°,90°] is proposed in this paper.

III.2. Dynamic case

III.2.1. Mean value μ_{dyn}

The means μ_{dyn} of the Gaussian distributions $N(\mu_{dyn}, \sigma_{dyn})$ that over-bound the raw code multipath ranging error $\varepsilon_{\text{code multipath}}(t_k)$ in the impact zone of a 10m and of a 20m metallic building are provided in Fig.12 and 13, respectively.

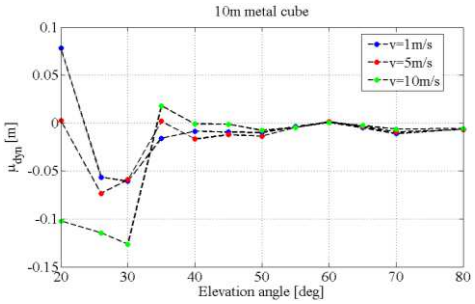

Figure 12: μ_{dyn} as a function of the elevation angle – impact zone of a 10m metallic cube

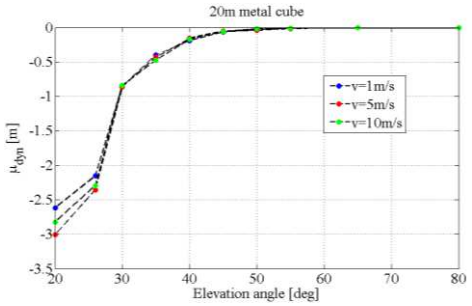

Figure 13: μ_{dyn} as a function of the elevation angle – impact zone of a 20m metallic cube

Note that, for low elevation angles, the mean μ_{dyn} is from few dm up to few m. An interpretation of the causes of these non-zero means is provided in Section **III.1.1**. More specifically, these non-zero mean values are due to the impact of the ground on $b_{A/C+ground+obs}$ and on the shape of $b_{A/C+ground+obs}$ in the direction orthogonal to the façade of large buildings.

Note also that the means observed in the dynamic cases are highly negative and larger in absolute values than the means observed in the static case (Fig. 8 and 9). This can be interpreted as follows. From **APPENDIX B** and Section **III.1.1**, at low elevation angles, and in the impact zone of large obstacles, the code multipath ranging errors $b_{A/C+ground+obs}$ presents sharp positive peaks (few m high) along the direction orthogonal to the façade. The rest of the errors in this direction are negative. The variations of the code multipath ranging errors in steady state are smoothed thanks to the aircraft dynamic [6]. Hence, the positive peaks present at low elevation and in the impact of large obstacles, such as at 20° elevation and in the impact zone of a 20m metallic building, are smoothed in the dynamic case. As a result of the smoothing of the high positive peaks, the mean of the raw and smoothed code multipath ranging errors become

negative, especially in the impact zone of the 20m metallic building, where μ_{dyn} reaches -3m.

III.2.2. Standard deviation value σ_{dyn}

The standard deviations σ_{static} of the Gaussian distributions $N(\mu_{dyn}, \sigma_{dyn})$ that over-bound the raw code multipath ranging errors $\varepsilon_{\text{code multipath}}(t_k)$ in the impact zone of a 10m metallic building and of a 20m metallic building are provided in Fig. 14 and 15, respectively.

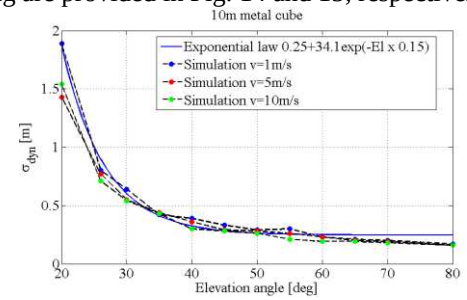

Figure 14: σ_{dyn} as a function of the elevation angle – impact zone of a 10m metallic cube

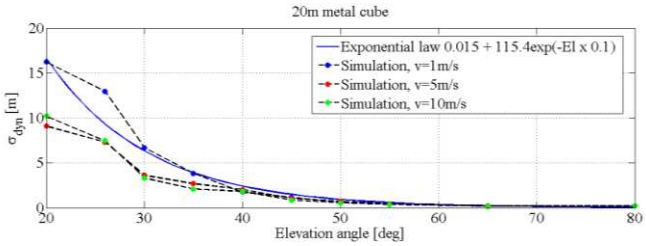

Figure 15: σ_{dyn} as a function of the elevation angle – impact zone of a 20m metallic cube

Note that the evolution of σ_{dyn} as a function of the elevation angle is fitted by an exponential function that has the following shape:

$$\sigma_{\text{dyn,exp fitting}}(\text{El}) = a_0 + a_1 . \exp(-\text{El}. a_2) \qquad \textbf{Eq.7}$$

where a_0, a_1, a_2 are real values that depend on the type of obstacle and on the speed of the aircraft in the impact zone. In this paper, a_0, a_1, a_2 have been evaluated based on the highest value of σ_{dyn} over all tested speeds at each elevation angle. The exponential fitted curves are depicted in blue in Fig. 14 and 15. a_0, a_1, a_2 coefficients are provided in Table 4 for metallic, concrete and glass obstacles.

Table 4: coefficients of the exponential laws that fit the values of σ_{dyn} obtained by simulations (1st line: unsmoothed case, 2nd line: 100s smoothed case)

	Metallic obstacles			Concrete obstacles			Glass obstacles		
Size	1	10	20	1	10	20	1	10	20
[m]									
a_0	0.07 0.07	0.25 0.07	0.015 0.06	0.03 0.01	0.08 0.05	0.36 0.06	0.03 0.03	0.07 0.05	0.3 0.09
a_1	2.3 1.1	34.1 1.3	115.4 95.6	0.91 0.2	35.2 2.83	428.5 29.2	1.7 1.06	13.3 1.8	191.4 122.0
a_2	0.11 0.08	0.15 0.07	0.10 0.15	0.10 0.07	0.19 0.14	0.21 0.16	0.11 0.09	0.11 0.10	0.14 0.19

From Fig. 14, 15 and From Table 4, the value of σ_{dyn} for a fixed elevation angle is smaller for the 10m metallic obstacle than for the 20m metallic obstacle. An interpretation of this observation is provided in Section **III.1.2**.

The aircraft speed in the impact zone impacts the value of σ_{dyn}, especially for elevation angles below 30°. For low elevation angles, σ_{dyn} is similar for 5m/s and 10m/s but is strongly increased for 1m/s. This is because the relatively high dynamic of the aircraft at 5m/s and 10m/s allows strongly reducing the error variations in the impact zone. This reduction of error variations also explains why, at low elevation angles, σ_{dyn} is quasi systematically lower than σ_{static}.

From Table 4, σ_{dyn} in the smoothed case is always lower than σ_{dyn} in the unsmoothed case for the same elevation angle and kind of obstacle. Numerically, for a 20m metallic obstacle, σ_{dyn} in the smoothed case is in average 4 times lower than in the unsmoothed case. Since the smoothed error determined in the impact zone of the obstacle at time t_k depends on the past errors affecting the pseudo range at time t_n, $n < k$ and $t_k - t_n \leq T_{smooth}$, some of the smoothed errors in the impact zone depend on the errors that affect the aircraft before entering into the impact zone. Thus, it is important to precise that the smoothed errors have been determined assuming that the pseudo range measurement is only affected by multipath from the ground and from the aircraft structure before entering into the impact zone.

CONCLUSION AND FUTURE WORKS

In this paper, we have analyzed the impact of multipath from the aircraft structure, from the ground, and from obstacles surrounding the airborne antenna on the GPS L1 C/A raw and smoothed code pseudo range measurements in static and dynamic conditions. In the following, the obtained results are summarized and future works are proposed.

In the static configuration, the raw and smoothed code multipath ranging errors are time-dependent. They converge to the DLL output steady state code multipath ranging error. In the case of a pseudo range measurement affected by multipath from the ground and from the aircraft structure, this error, denoted as $b_{A/C+ground}$, is constant at the scale of the airport and mainly depends on the satellite elevation angle. It reaches a few mm at zenith

and a few dm at low elevation angles (below 35°). If the pseudo range measurement is also affected by multipath from a single obstacle of the airport environment, the DLL output steady state code multipath ranging error strongly depends on the true position of the GPS airborne antenna in the impact zone of the obstacle. The distribution of this error in the impact zone is over-bounded by a Gaussian distribution. The distribution parameters depend on the elevation angle, on the aircraft and façade orientations in the airport and on the kind of obstacle. For an aircraft centerline and an illuminated façade parallel and orthogonal to the GNSS signal respectively, the following results have been obtained. The distribution is roughly zero-mean (from few mm up to few cm) for elevation angles above 35° and which is non-zero mean (up to few dm) for elevation below 35°. Below 35° elevation, the mean values are lower for obstacles with a size significantly larger than 15m (high negative values up to few dm) than for smaller obstacles. The sigma values of the Gaussian distribution mainly depend on the elevation angle and on the type of obstacle and reaches few m at low elevations and for large metallic obstacles (20m obstacles). For a fixed obstacle, the variations of the sigma values as a function of the elevation follow an exponential law. For a fixed elevation angle, the sigma value increases when the size of obstacle increases.

For the dynamic case, this paper focuses on constant speed straight line trajectories. Even if first observations reveal that the exact shape of the trajectory in the impact zone is not likely to induce major changes in the error model results, further validations are needed to extend the proposed model to curved trajectories. The paper assumes that the satellite is static during the trajectory. Indeed, the angular variation of the satellite during the trajectory (from few seconds up to few minutes) is considered as non-significant, and is thus neglected. In the case of a pseudo range measurement affected by multipath from the ground and from the aircraft structure, the code multipath ranging error along the trajectory is an error that is constant in the time domain. The value of this error is $b_{A/C+ground}$. Further details about the factors influencing this error are provided in the second paragraph of this Section. If the pseudo range measurement is also affected by multipath from a single obstacle of the airport environment along the trajectory, raw and smoothed code multipath ranging errors along the trajectory are over-bounded by a Gaussian distribution. The distribution parameters depend on the elevation angle, the façade orientation in the airport, the kind of obstacle and the aircraft speed. For an illuminated façade orthogonal to the GNSS signal, the mean and sigma values of the distribution are compared to the values obtained in the static configuration. At low elevation angles (below 35°), and for a fixed obstacle, the non-zero mean values observed in the static case are decreased and shifted into the negative domain by the aircraft dynamics. They reach few dm up to few m in the negative domain for a 20m metallic building at 20° elevation angle. For a fixed elevation angle and obstacle, the sigma values are also decreased by the aircraft speed, especially for speeds equal and greater than 5m/s. The sigma values obtained for aircraft speeds in the range [5m/s,10m/s] are similar. Sigma values for an aircraft speed of 1m/s are higher, especially for elevation angles below 35°.

In this paper, models of ranging errors due to multipath from the ground, from the aircraft structure, and from a single obstacle present in the airport environment are presented in both static and dynamic configurations. Future works can be organized as follows. The coefficients that parameterized the derived models depend on the aircraft orientation (for static case), on the obstacle, on the façade orientation, on the aircraft speed and on the elevation angle. The first perspective is to reduce the number of parameters by analyzing the influence of each parameter and isolating parameters that strongly influence the error models. As an example, the influence of the orientation of the illuminated façade on the error model parameters has to be investigated. The second perspective is to simplify the 3D airport model. The influence of the obstacle characteristics (such as the exact material) on the error model has also to be investigated in order to distinguish which elements of the obstacles cannot be precisely represented. Obstacles inducing non-critical errors in terms of accuracy and integrity will also be identified and removed from the 3D airport environment.

APPENDIX A

The smoothed pseudo range measurement at epoch $\mathbf{t_k}$ is given as follows (A.1):

$$\hat{\rho}(t_k)_{smoothed} = (1-\beta)\left[\hat{\rho}(t_{k-1})_{smoothed} + \hat{\rho}(t_k)_{phase} - \hat{\rho}(t_{k-1})_{phase}\right] + \beta\hat{\rho}(t_k)_{code}$$

where:

- β is the smoothing constant ($0 < \beta < 1$): $\beta = \frac{T_s}{T_{smooth}}$
- $\hat{\rho}(t_k)_{phase}$ is the phase pseudo range estimate between the airborne GNSS antenna and satellite "i". Assuming that assumed that the phase measurement is only affected by the phase ambiguity term, $\hat{\rho}(t_k)_{phase} = \rho(t_k) + \lambda_{L1}A$.
- $\hat{\rho}(t_k)_{code}$ is the code pseudo range estimate between the airborne GNSS antenna and satellite "i". Assuming that code measurement is only affected by the code multipath ranging error, $\hat{\rho}(t_k)_{code} = \rho(t_k) + \varepsilon_{code\ multipath}(t_k)$
- A is the phase ambiguity term,
- λ_{L1} is the wavelength of the RF carrier,
- $\rho(t_k)$ is the topocentric distance between the receiver at time of reception and satellite at time of transmission.

Assuming that the phase ambiguity term is constant between epoch t_{k-1} and epoch t_k, and rearranging Equation (A.1), we get (A.2):

$$\hat{\rho}(t_k)_{smoothed} - \rho(t_k) = (1-\beta)[\hat{\rho}(t_{k-1})_{smoothed} - \rho(t_{k-1})] + \beta[\varepsilon_{code\ multipath}(t_k)]$$

Let's state [16]:

$$\varepsilon_{smoothed\ multipath}(t_k) = \hat{\rho}(t_k)_{smoothed} - \rho(t_k)$$

Equation (A.2) becomes (A.3):

$$\varepsilon_{smoothed\ multipath}(t_k) = (1-\beta)[\varepsilon_{smoothed\ multipath}(t_{k-1})] + \beta\varepsilon_{code\ multipath}(t_k)$$

Assuming that $T_{smooth} \gg T_s$, Equation (A.3) can be written as (A.4):

$$\frac{d\varepsilon_{smoothed\ multipath}(t)}{dt} = -\frac{1}{T_{smooth}}\varepsilon_{smoothed\ multipath}(t) + \frac{1}{T_{smooth}}\varepsilon_{code\ multipath}(t)$$

The solutions of Equation (A.4) are [16] (A.5):

$$\varepsilon_{smoothed\ multipath}(t) = \exp\left[-\frac{t}{T_{smooth}}\right]\left[c + \int_{u=0}^{t}\exp\left[\frac{u}{T_{smooth}}\right]\frac{1}{T_{smooth}}\varepsilon_{code\ multipath}(u)du\right]$$

From Section **II.1**, in steady state (A.6):

$$\varepsilon_{code\ multipath}(t) = b$$

So we get:

$$\varepsilon_{code\ multipath}(t) = \exp\left[-\frac{t}{T_{smooth}}\right]\left[c + b\left[\exp\left[\frac{t}{T_{smooth}}\right] - 1\right]\right]$$

where $c = \varepsilon_{multipath\ smoothed\ ranging\ error}(t=0)$.
Simulations have shown that Equation (A.6) is also valid during the transient state.

APPENDIX B

Let's simplify the problem by assuming that the airborne antenna receives 2 signals: the direct signal characterized by a code delay τ_{direct}, and only one signal reflected from the façade and characterized by a code delay $\tau_{reflect,2}$. At point $x_n, x_n \in [x_0, x_f]$ of a segment [AB] orthogonal to the façade of the building, the Early minus Late Power discriminator output is given by:

$$D_{output} = (I_E(x_n)^2 + Q_E(x_n)^2) - (I_L(x_n)^2 + Q_L(x_n)^2) \quad \textbf{Eq.(B.1)}$$

where I_E, I_L, Q_E, Q_L are the in phase and quadrature Early and Late correlator outputs given by:

$$\begin{aligned} I_E(x_n) &= \alpha_0 K\left(\varepsilon_\tau + \frac{C_s}{2}\right) + \alpha_2 K\left(\varepsilon_\tau + \frac{C_s}{2} + \Delta\tau_2(x_n)\right)\cos\left(\Delta\phi_2(x_n)\right) \\ Q_E(x_n) &= \alpha_2 K\left(\varepsilon_\tau + \frac{C_s}{2} + \Delta\tau_2(x_n)\right)\sin\left(\Delta\phi_2(x_n)\right) \\ I_L(x_n) &= \alpha_0 K\left(\varepsilon_\tau - \frac{C_s}{2}\right) + \alpha_2 K\left(\varepsilon_\tau - \frac{C_s}{2} + \Delta\tau_2(x_n)\right)\cos\left(\Delta\phi_2(x_n)\right) \\ Q_L(x_n) &= \alpha_2 K\left(\varepsilon_\tau - \frac{C_s}{2} + \Delta\tau_2(x_n)\right)\sin\left(\Delta\phi_2(x_n)\right) \end{aligned} \quad \textbf{Eq.(B.2)}$$

where:

- K is the autocorrelation function of the GPS L1 C/A signal,
- ε_τ is the code delay estimate error at the DLL output at $x = x_n$,
- $\Delta\phi_2(x_n)$ and $\Delta\tau_2(x_n)$ are the relative code delay and relative phase between the echo and direct signals at $x = x_n$.

By considering the analytical expression of the autocorrelation function of GPS L1 C/A signals, and by remarking that a stable lock point is reached when $D_{output} = 0$, Equation (B.2) in Equation (B.1) leads to:

$$\varepsilon_\tau = -\Delta\tau_2(x_n)\frac{1 + \alpha\cos\left(\Delta\phi_2(x_n)\right)}{\alpha^2 + 1 + 2\alpha\cos\left(\Delta\phi_2(x_n)\right)}$$

where $\alpha = \frac{\alpha_0}{\alpha_2} \in [0,1]$ is the amplitude of the echo signal with respect to the amplitude of the direct signal. Note that this expression does not take into account the presence of the front-end filter and its impact on the correlation function nor the impact of the phase multipath ranging error on the correlator outputs. Moreover, Equation (C.3) is valid for $\Delta\tau_2(x_n) \in \left[0, \frac{C_s}{2}\right]$, that is to say when the distance between the illuminated façade and the airborne antenna located on [AB] is less than 73m. From section **II.1.2.2.1:**

$$\Delta\tau_2(x_n) = 2\tau_{A\to obs} + \frac{2}{c}(x_n - x_0)$$

$$\Delta\phi_2(x_n) = -2\pi f_{L1}\Delta\tau_2(x_n)$$

When a stable point is reached, $c.\varepsilon_\tau = b_{obs}$. Let's plot b_{obs} as a function of x_n assuming that $\tau_{A\to obs} = 0s$ and that $x_0 = 0m$ for $\alpha = 0.1$ and $\alpha = 0.9$ in Fig.B.1 and B.2, respectively.

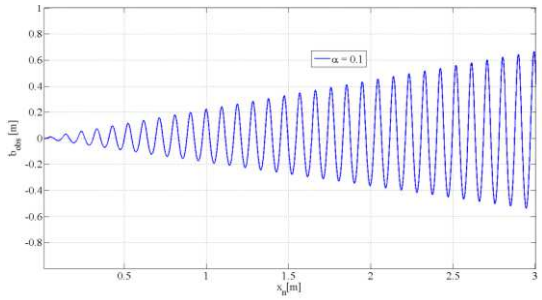

Figure B.1 : b_{obs} along a segment orthogonal to the façade [AB] for $\alpha = 0.1$

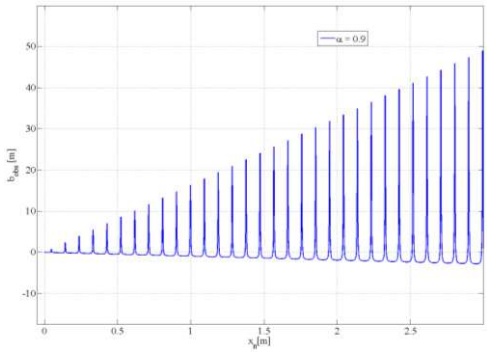

Figure B.2 : b_{obs} along a segment orthogonal to the façade [AB] for $\alpha = 0.9$

From Fig. B.2, the pattern of b_{obs} along [AB] in the presence of strong echo signals ($\alpha = 0.9$ in this Figure) is not symmetrical with respect to zero and has a "U-shape". b_{obs} presents sharp positive peaks and the rest of the values are negative values. The median of the code multipath ranging errors b_{obs} on [AB] is thus negative. It is noted that this phenomena has also been underlined for a 1 chip correlator spacing and for an Early minus Late discriminator in [12].

APPENDIX C

Fig. C.1 and C.2 show the power of the field scattered by a 1m metallic obstacle and by a 20m metallic obstacle 8.10m above the ground. From these Figures, in front of the 1m obstacle, the power of the scattered field is about 30 dB less than in front of the 20m obstacle.

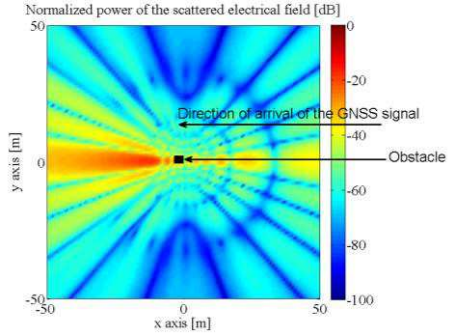

Figure C.1: Normalized power [dB] of the field scattered by a 1m metallic obstacle 8.10m above the ground

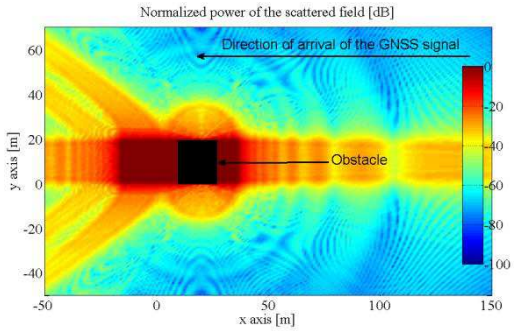

Figure C.2: Normalized power of the field [dB] scattered by a 20m metallic obstacle 8.10m above the ground

APPENDIX D

Let's consider a 200m long segment [AB] orthogonal to the façade of a 15m metallic building. A GNSS signal arrives orthogonally to the façade of the building with an elevation of 5°. [AB] is located in the impact zone of the façade. Along [AB], the amplitude of the direct and first echo signal coming from the façade are computed as follows [6]:

$$\alpha_0 = \frac{\vec{E}_0 . \overrightarrow{h_{eff}}}{V_0} \text{ and } \alpha_1 = \frac{\vec{E}_1 . \overrightarrow{h_{eff}}}{V_0}$$

where:

- $\overrightarrow{h_{eff}}$ is the effective height of the antenna which can be decomposed into Right Hand Circular Polarization (RHCP) and Left Hand Circular Polarization (LHCP) components as: $\overrightarrow{h_{eff}} = \gamma_R \overrightarrow{e_R} + \gamma_L \overrightarrow{e_L}$. Note that $\overrightarrow{h_{eff}}$ depends on the direction of arrival of the incoming electrical field,
- $\vec{E}_0$ is the incoming electrical field of the direct path that reaches the receiver antenna,
- $\vec{E}_1$ is the incoming electrical field of the 1st echo path from the façade that reaches the receiver antenna,
- $\overrightarrow{e_R}$ is the right polarization unit vector,
- $\overrightarrow{e_L}$ is the left polarization unit vector,
- γ_R is the right polarization component,
- γ_L is the left polarization component,
- V_0 is the voltage at the output of the antenna obtained for an ideal configuration in which the antenna is perfect and the scene is empty [6].

The polarization of the real antenna at low elevation angles is roughly linear (see section **III.1.2**). For this reason, even if the power of the direct electrical field is larger than the power of the reflected electrical field along [AB], at very low elevation angles, and in the impact zone of obstacles inducing powerful reflected fields in the impact zone, α_1 is larger than the amplitude of the direct signal α_0 and the GNSS receiver tracks the 1st echo signal. This can be visualized in Fig. D.1 that shows the code ranging error $b_{A/C+ground+obs}$ along [AB]. Between

5m and 80 m from the façade, the GNSS receiver estimates the 1st echo code delay that increases linearly along [AB]. Hence, the code delay error, that corresponds to the difference between the true code delay and the estimated code delay, increases linearly along [AB] in the negative domain until d= 80m. At this point, α_1 becomes smaller than α_0 mainly because of the low power of the electrical reflected field that decreases when the distance to the obstacle increases.

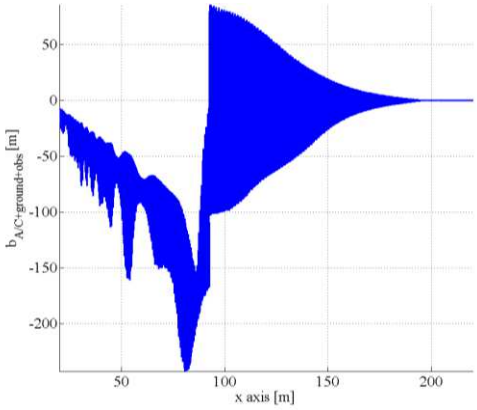

Figure D.1: $b_{A/C+ground+obs}$ along a segment [AB] orthogonal to the façade of a 15m metallic building and in the impact zone – Elevation angle = 5°

ACKNOWLEDGEMENT

I would like to acknowledge Quentin TESSIER, ENAC Master Student in electronics, for his help in running the simulations needed for Part III.

REFERENCES

[1]: "Annex 10 to the Convention on International Civil Aviation, Aeronautical Telecommunications, Volume I Radio Navigation Aids", International Civil Aviation Organization, Sixth Edition, July 2006.

[2]: "A study of severe multipath errors for the proposed GBAS airport surface movement application", Y.S.Park, S.Pullen, P. Enge, Stanford University, ION GNSS 2010.

[3]: "LAAS operations in support of airport surface movement, guidance, control and surveillance: initial test results", M. Braasch, M. DiBenedetto, S.Braasch, R. Thomas, Ohio University, IEEE 2000.

[4]: "11th Air Navigation Conference, Report of committee B to the conference on Agenda Item 6, recommendation 6/1", Montreal, 22 September to 3 October 2003.

[5]: "Understanding GPS Principles and Applications, Second Edition", E.D. Kaplan, C. J. Hegarty, 2006

[6]: "Development of a hybrid deterministic-statistical GPS multipath simulator for airport navigation, PhD dissertation", A. Chen, Université de Toulouse, 2010

[7]: "Channel characterization for spread spectrum satellite communications", A. Jahn, H.Bischl, G. Heiss, in Proceedings on IEEE Fourth International Symposium on Spread Spectrum Techniques and Applications, 1221-1226, 1996

[8]: "Minimum Operational Performance Standards for Global Positioning System (GPS) / Wide Area Augmentation System Airborne Equipment, DO 229D", Radio Technical Commission for Aeronautics, Special Committee 159, December 2006

[9]: "Minimum aviation system performance standards for the Local Area Augmentation System (LAAS), DO 245A", Radio Technical Commission for Aeronautics, Special Committee 159, December 2004

[10]: "Minimum Operational Performance Standards for Global Positioning System (GPS) / Aircraft Based Augmentation System Airborne Equipment, DO 316", Radio Technical Commission for Aeronautics, Special Committee 159, April 2009

[11]: "Characterization of the Earth-Surface Multipath Error for Aircraft GPS Receivers", Z. Zhu, F. van Graas, ION GNSS 18th International Technical Meeting of the Satellite Division, Long Beach, CA, September 2005

[12]: "Mitigation of GPS Code and Carrier Phase Multipath Effects Using a Multi-Antenna System, PhD dissertation», J. K. Ray, University of Calgary, 2000

[13] : « Impact des multitrajets sur les performances des systèmes de navigation par satellite : Contribution à l'amélioration de la précision de localisation par modélisation bayésienne, PhD dissertation », D. F. Nahimana, Ecole Centrale de Lille, 2011

[14]: "Defining Pseudorange Integrity. Overbounding", B. DeCleene, ION GPS 2000, Salt Lake City, UT, September 2000

[15]: "The role of the Global Navigation Satellite System (GNSS) in supporting airport surface operations, DO 247", Radio Technical Commission for Aeronautics, Special Committee 159, January 1999

[16]: "The Effects of Large Ionospheric Gradients on Single Frequency Airborne Smoothing Filters for WAAS and LAAS", T. Walter, S. Datta-Barua, J. Blanch, P. Enge, Proceedings of the 2004 National Technical Meeting of The Institute of Navigation, January 2004

[17]: “A proposed formula to inflate the sigma during the smoothing convergence”, M. Hernandez-Pajares, M. Juan, J. Sanz, P. Ramos, ESTB/EGNOS data collection and evaluation 12th WG meeting, Gatwick airport, December 2004

[18]: “Optimization of demodulation performance of the GPS and GALILEO navigation messages, PhD dissertation”, A. Garcia Pena, Université de Toulouse, 2010

[19]: “Digital Communications”, J.G. Proakis, McGraw-Hill, 2001

[20]: “Channel characterization for spread spectrum satellite communications”, A. Jahn, H.Bischl, G. Heiss, in Proceedings on IEEE Fourth International Symposium on Spread Spectrum Techniques and Applications, 1221-1226, 1996

[21]: “Development of a GPS deterministic multipath simulator for a, efficient computation of the positioning errors”, A. Chen, A. Chabory, A-C Escher, C. Macabiau, 22nd International Meeting of the Satellite Division of The Institute of Navigation, September 2009